Structural Bases for Inhibitor Binding and Catalysis in Polyamine Oxidase[†,‡]

Claudia Binda,[§] Riccardo Angelini,[||] Rodolfo Federico,[||] Paolo Ascenzi,[||] and Andrea Mattevi*[,§]

Dipartimento di Genetica e Microbiologia, Università di Pavia, Via Abbiategrasso 207, I-27100 Pavia, Italy, and Dipartimento di Biologia, Università "Roma Tre", Viale Guglielmo Marconi 446, I-00146 Roma, Italy

Received December 4, 2000; Revised Manuscript Received January 11, 2001

ABSTRACT: Polyamine oxidase (PAO) carries out the FAD-dependent oxidation of the secondary amino groups of spermidine and spermine, a key reaction in the polyamine catabolism. The active site of PAO consists of a 30 Å long U-shaped catalytic tunnel, whose innermost part is located in front of the flavin ring. To provide insight into the PAO substrate specificity and amine oxidation mechanism, we have investigated the crystal structure of maize PAO in the reduced state and in complex with three different inhibitors, guazatine, 1,8-diaminooctane, and N^1-ethyl-N^{11}-[(cycloheptyl)methyl]-4,8-diazaundecane (CHENSpm). In the reduced state, the conformation of the isoalloxazine ring and the surrounding residues is identical to that of the oxidized enzyme. Only Lys300 moves away from the flavin to compensate for the change in cofactor protonation occurring upon reduction. The structure of the PAO·inhibitor complexes reveals an exact match between the inhibitors and the PAO catalytic tunnel. Inhibitor binding does not involve any protein conformational change. Such lock-and-key binding occurs also in the complex with CHENSpm, which forms a covalent adduct with the flavin N5 atom. Comparison of the enzyme complexes hints at an "out-of-register" mechanism of inhibition, in which the inhibitor secondary amino groups are not properly aligned with respect to the flavin to allow oxidation. Except for the Glu62−Glu170 pair, no negatively charged residues are involved in the recognition of substrate and inhibitor amino groups, which is in contrast to other polyamine binding proteins. This feature may be exploited in the design of drugs specifically targeting PAO.

The natural polyamines putrescine [$NH_2(CH_2)_4NH_2$], spermidine [$NH_2(CH_2)_3NH(CH_2)_4NH_2$], and spermine [$NH_2(CH_2)_3NH(CH_2)_4NH(CH_2)_3NH_2$] are ubiquitous in living organisms, being essential for cell growth and differentiation. Their biological role is being extensively investigated, and the number of known processes that involve these linear polycationic molecules is continuously increasing. The intracellular concentration of polyamines is finely regulated through pathways for their synthesis, degradation, and uptake (*1*−*3*).

Polyamine oxidase (PAO)[1] is a FAD-dependent enzyme that catalyzes the oxidation of the secondary amino groups of spermine, spermidine, and their acetylated derivatives (*4*, *5*). The reaction is part of the ubiquitous pathway for polyamine degradation. The nature of the products of PAO reactions depends on the enzyme source. Animal PAO oxidizes preferentially N^1-acetylspermidine and N^1-acetylspermine into putrescine and spermidine, respectively, in addition to 3-acetamidopropionaldehyde (*5*). In plants and bacteria, PAO converts spermidine and spermine into 4-aminobutyraldehyde and 3-(aminopropyl)-4-aminobutyraldehyde, respectively, in addition to 1,3-diaminopropane (Figure 1) (*4*, *6*).

The interest in polyamine metabolism has increased with the discovery that some polyamine analogues exhibit antitumoral effects on a number of cell lines (*2*). Various polyamine analogues display antineoplastic activity in vitro and are currently being evaluated in clinical trials (*7*). Therefore, progress in the analysis of the metabolism of these compounds is a promising route for the design of new drugs (*8*). Although the precise mechanism of the cytotoxic activity of polyamines is unknown, it has been noticed that the accumulation of polyamine analogues leads to DNA fragmentation and cell death by apoptosis (*9*, *10*). In particular, some polyamine analogues, such as N^1-ethyl-N^{11}-[(cyclopropyl)methyl]-4,8-diazaundecane[2] (CHENSpm; Figure 1), may induce programmed cell death by increasing the rates

[†] This research was supported by grants from Consiglio Nazionale delle Ricerche of Italy (target-oriented project on biotechnology) and from Agenzia Spaziale Italiana.

[‡] Atomic coordinates and structure factors have been deposited in the Protein Data Bank with accession codes 1h81 and r1h81sf for reduced PAO, 1h82 and r1h82sf for the PAO·guazatine complex, 1h83 and r1h83sf for the PAO·1,8-diaminooctane complex, 1h84 and r1h84sf for the PAO·CHENSpm complex at pH 4.6, and 1h86 and r1h86sf for the PAO·CHENSpm complex at pH 7.0.

* To whom correspondence should be addressed: Department of Genetics and Microbiology, University of Pavia, Via Abbiategrasso 207, I-27100 Pavia, Italy. Phone: +39-0382-505560. Fax: +39-0382-528496. E-mail: mattevi@ipvgen.unipv.it.

[§] Università di Pavia.

[||] Università "Roma Tre".

[1] Abbreviations: PAO, polyamine oxidase; FAD, flavin adenine dinucleotide; CHENSpm, N^1-ethyl-N^{11}-[(cycloheptyl)methyl]-4,8-diazaundecane; MDL72527, *N*,*N*′-bis(2,3-butadienyl)-1,4-butanediamine; BES, *N*,*N*-bis(2-hydroxyethyl)-2-aminoethanesulfonic acid; rmsd, root-mean-square deviation; NCS, noncrystallographic symmetry; PDB, Protein Data Bank.

[2] The IUPAC name of CHENSpm is (3-{[3-({3-[(cycloheptylmethyl)-amino]propyl}amino)propyl]amino}propyl)ethylamine. CHENSpm and N^1-ethyl-N^{11}-[(cycloheptyl)methyl]-4,8-diazaundecane are the acronym and the name, respectively, being generally used in the literature.

10.1021/bi002751j CCC: $20.00
Published on Web 02/08/2001

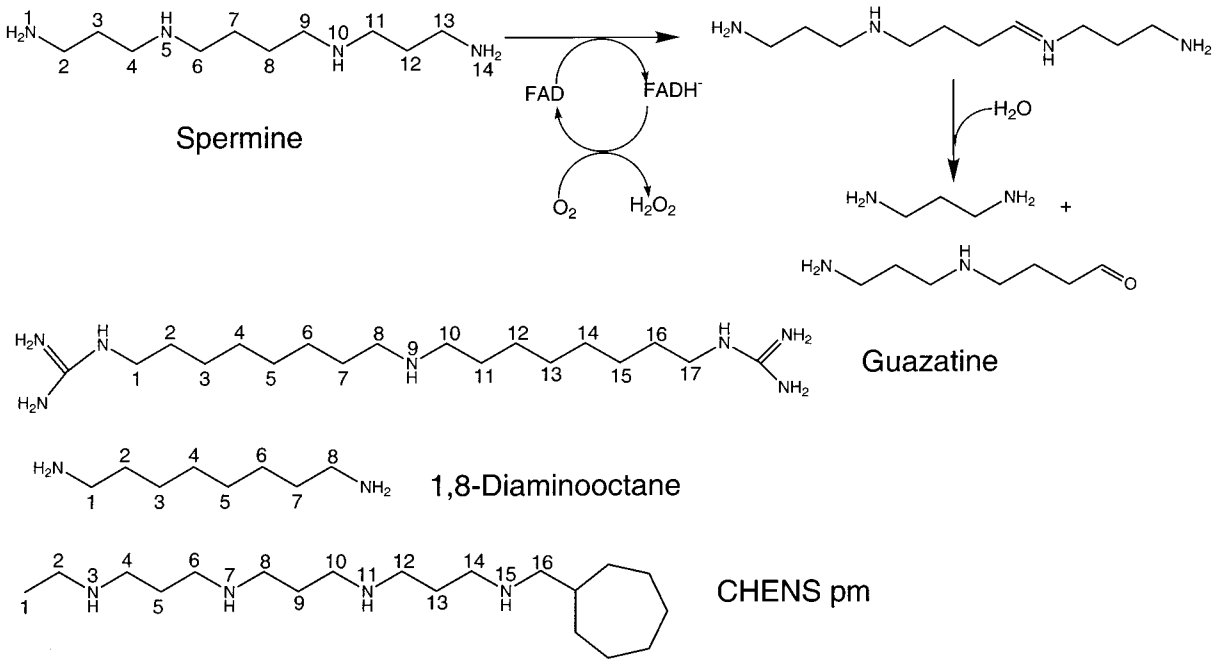

FIGURE 1: Reaction scheme for spermine oxidation catalyzed by maize PAO (top) and chemical structure and atomic numbering of the PAO inhibitors guazatine, 1,8-diaminooctane, and CHENSpm used in the crystallographic analysis (bottom).

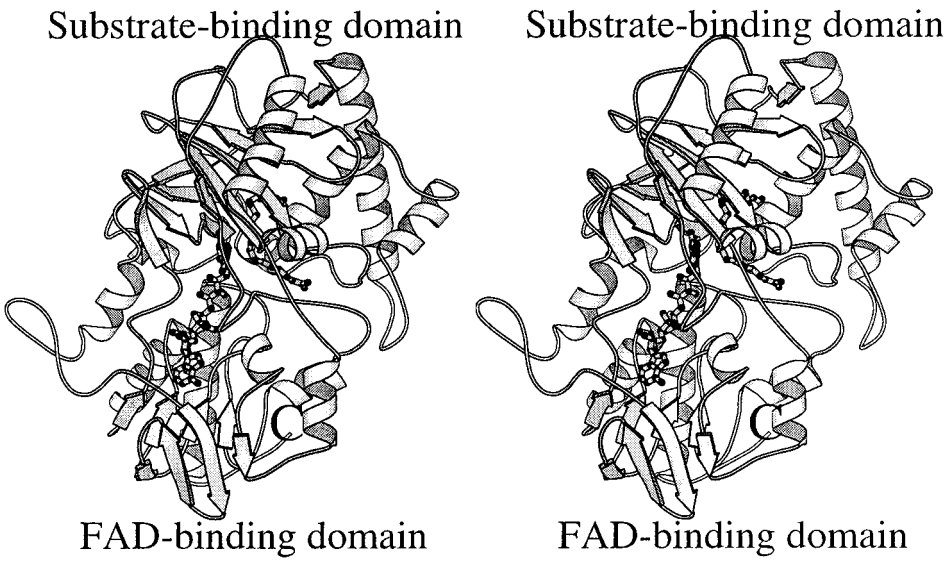

FIGURE 2: Molscript stereodrawing of PAO (chain C) in complex with guazatine. The inhibitor and the FAD molecules are shown in ball-and-stick representations. The trace of the inhibitor closely follows the path of the U-shaped catalytic tunnel.

of polyamine catabolism and consequent production of toxic H_2O_2 (*11*). Moreover, it has been suggested that PAO is involved in programmed cell death in plants (*12*).

Maize (*Zea mays* L.) PAO represents the first PAO of known primary and tertiary structure (*13*, *14*). The crystal structure of maize PAO had been determined by X-ray diffraction at 1.9 Å resolution in the native oxidized state and in complex with the inhibitor *N*,*N*′-bis(2,3-butadienyl)-1,4-butanediamine (MDL72527) (*14*). The X-ray analysis revealed that the enzyme structure consists of two domains, a FAD-binding domain showing the typical Rossmann fold topology and a substrate binding domain, comprising a central β-sheet flanked by α-helices (Figure 2). This overall folding topology is similar to that of many other flavoenzymes (*15*). A prominent feature of the PAO structure is a 30 Å long U-shaped catalytic tunnel located at the interface between the two domains. The innermost part of the tunnel is positioned in front of the flavin ring and forms the catalytic center. The tunnel is lined mainly by aromatic side chains and carbonyl and carboxylate oxygen atoms, which are able to form CH···O H-bonds with the active site ligands. A ring of glutamate and aspartate side chains surrounding one of the two tunnel openings may help to steer the substrate toward the tunnel interior.

Here, we report the crystal structure of complexes of maize PAO and three different inhibitors. The aim of this study is the characterization of the structural bases of inhibitor and substrate binding and specificity in PAO, a prerequisite for the design of inhibitors targeting enzymes involved in polyamine metabolism. For these purposes, the symmetrical competitive inhibitors guazatine[3] and 1,8-diaminooctane

[3] Guazatine is 1,1′-iminodi(octamethylene)diguanidine triacetate (Figure 1).

Table 1: Data Collection and Refinement Statistics[a]

	reduced state	CHENSpm (pH 4.6)	CHENSpm (pH 7.0)	1,8-diaminooctane	guazatine
resolution (Å)	2.1	2.0	2.0	1.9	1.9
cell axes *a*, *c* (Å)	181.77, 277.53	184.04, 280.80	184.29, 279.61	184.69, 282.22	184.97, 282.24
I/σ[b]	35.1 (10.3)	15.4 (5.6)	13.3 (4.9)	12.1 (3.8)	11.2 (2.2)
no. of observations	1527497	617266	599120	774835	677712
no. of unique reflections	156392	172552	174933	215494	207570
completeness (%)[b]	99.8 (99.2)	93.5 (90.8)	94.9 (93.2)	97.9 (87.9)	94.3 (81.6)
R_{sym} (%)[b,c]	7.0 (17.6)	7.0 (21.4)	9.4 (19.8)	8.1 (32.8)	10.1 (38.0)
no. of protein atoms	11389	11389	11389	11389	11389
no. of waters	724	745	791	734	746
no. of ligand atoms	−	42	42	60	69
average *B* (Å^2)					
chain A	19.6	15.9	15.3	15.4	18.4
chain B	18.0	14.7	13.3	13.6	17.7
chain C	16.7	13.7	11.9	12.8	15.4
ligand	-	34.7	33.2	19.7	40.0
water	23.7	20.4	19.0	21.1	24.3
rmsd[d] (Å)					
chain A and chain B	0.43	0.51	0.54	0.52	0.47
chain A and chain C	0.32	0.32	0.40	0.50	0.50
chain B and chain C	0.32	0.50	0.50	0.50	0.50
R_{factor} (%)[e]	19.1	18.9	18.4	19.6	19.9
no. of reflections for R_{free}	1570	1746	1745	2176	2107
R_{free}	23.5	22.7	22.9	23.7	23.1
rmsd for bond lengths (Å)[f]	0.009	0.009	0.010	0.009	0.011
rmsd for bond angles (deg)[f]	2.2	2.1	2.2	2.1	2.0

[a] No σ or low-resolution cutoff was applied. All measured data were used in the refinement. [b] The values for the highest-resolution shell are in parentheses. [c] $R_{sym} = \Sigma_h\Sigma_i|I(h) - I_i(h)|/\Sigma_h\Sigma_i I_i(h)$, where $I_i(h)$ and $I(h)$ are the *i*th and mean measurements of reflection *h*, respectively. [d] The rmsd values are for all NCS-related protein and FAD atoms. [e] *R*-factor $= \Sigma_h||F_o| - |F_c||/\Sigma_h|F_c|$, where F_o and F_c are the observed and calculated structure factors of reflection *h*, respectively. [f] The rmsds from the ideal values were calculated with the program TNT (*21*).

(Figure 1) were chosen, since they exemplify the ability of PAO to bind molecules that greatly differ in size, the chain of guazatine being 2 times longer than that of 1,8-diaminooctane. Moreover, the complex of PAO with CHENSpm (Figure 1) was investigated. CHENSpm is a member of a group of several asymmetrically alkylated inhibitors, which are presently being tested as potential antitumor agents (*7*, *11*). In particular, CHENSpm is peculiar in that it carries a bulky cycloheptyl terminal substituent. Finally, as a part of this study, the structure of PAO in the reduced state was determined.

EXPERIMENTAL PROCEDURES

Materials. All chemicals used in crystallization [sodium chloride, sodium phosphate, ammonium sulfate, sodium acetate, glycerol, and *N*,*N*-bis(2-hydroxyethyl)-2-aminoethanesulfonic acid] were from Sigma. Guazatine was provided by Rhòne-Poulenc (Agro, Italy). 1,8-Diaminooctane and spermine were from Sigma. CHENSpm was a generous gift of R. A. Casero, Jr. (University of Baltimore, Baltimore, MD), and was synthesized as reported previously (*16*).

Crystallization and Crystal Soaking. Maize PAO was purified and crystallized as previously reported (*17*). Briefly, crystals were grown by the hanging drop vapor diffusion method at 20 °C. Droplets containing 4 mg of enzyme/mL in 300 mM NaCl and 50 mM sodium phosphate buffer (pH 6.0) were equilibrated against a reservoir solution consisting of 42−50% saturated ammonium sulfate and 100 mM sodium acetate (pH 4.6). All PAO·inhibitor complexes were obtained by soaking at 20 °C for 24 h. Experiments were performed using the following ligands: guazatine, 1,8-diaminooctane, CHENSpm, and spermine. The soaking solutions consisted of 5 mM ligand, 55% saturated ammonium sulfate, and 100 mM sodium acetate buffer (pH 4.6). The complex with CHENSpm at pH 7.0 (Table 1) was obtained by using a soaking solution containing 100 mM *N*,*N*-bis(2-hydroxyethyl)-2-aminoethanesulfonic acid (BES) (pH 7.0) rather than sodium acetate (pH 4.6). PAO crystals have the typical bright yellow color of the oxidized flavin. Soaking in 1,8-diaminooctane and guazatine did not result in any change in the crystal color. Conversely, during soaking with spermine and CHENSpm, the yellow color of the crystals vanished. This process, indicative of flavin reduction, occurred in a few minutes in the case of soaking in the spermine containing solution, whereas it took several hours to be completed in the experiments with CHENSpm.

Data Collection, Crystallographic Refinement, and Model Analysis. For data collection, crystals were transferred into a cryoprotectant solution containing 5 mM ligand, 50% saturated ammonium sulfate, 25% (v/v) glycerol, and 100 mM sodium acetate buffer (pH 4.6) [100 mM BES (pH 7.0) for the PAO·CHENSpm complex at pH 7.0]. All X-ray diffraction experiments were performed at 100 K using standard cryocrystallographic techniques (*18*). Data were measured for reduced PAO at beam line BW7B at EMBL/DESY (Hamburg, Germany) using a MAR-IP345 and for the PAO complexes at beam line ID14-EH3 of the European Synchrotron Radiation Facility (Grenoble, France) using a MarCCD detector. The data were processed with MOSFLM (*19*) and programs of the CCP4 suite (*20*). Crystals of PAO·inhibitor complexes had a diffraction power comparable to that of the native oxidized crystals, allowing measurement of the diffraction data up to 1.9−2.1 Å resolution.

The crystals of PAO complexes were isomorphous to those of the native oxidized enzyme (*14*) (Table 1). They belong to space group $P6_522$ with three enzyme molecules in the

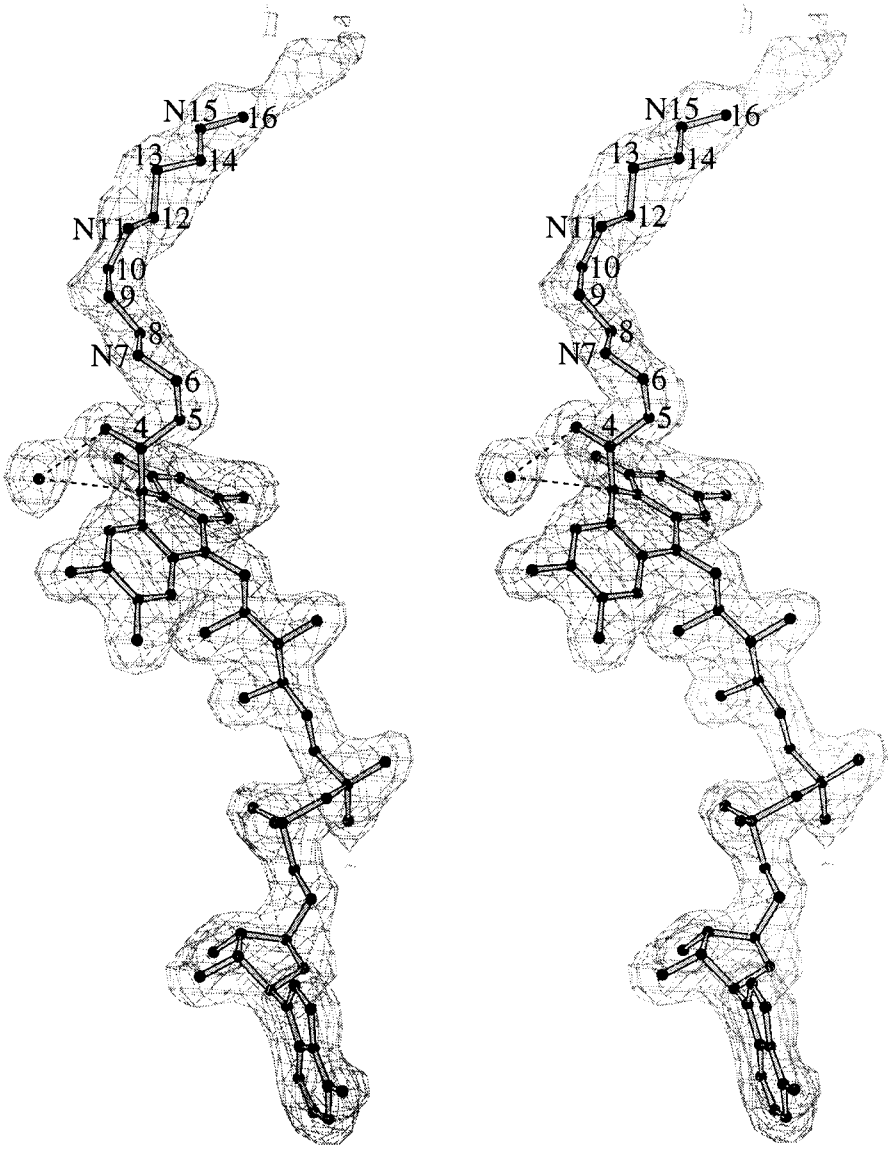

FIGURE 3: Stereoview of the final $2F_o - F_c$ map (chain C) of the covalent PAO·CHENSpm adduct at pH 4.6 (Table 1). The drawing also shows the water molecule H-bonded to the adduct hydroxyl group. At the terminus of the CHENSpm chain (C16), there is some residual electron density that is probably due to a partly ordered conformation of the cycloheptyl substituent (see the text). The contour level is 1.0σ. CHENSpm atoms are numbered as in Figure 1. With respect to Figure 2, the molecule has been rotated by 50° around an axis perpendicular to the plane of the drawing.

asymmetric unit. Atomic coordinates were refined by means of the least-squares refinement program TNT (*21*). In all experiments, the initial model used in refinement was that of the native unligated structure (*14*), deposited as entry 1b37 in the Protein Data Bank (*22*). All measured data were employed, without applying any low-resolution or σ cutoff. Throughout refinement, tight NCS restraints were applied to the three crystallographically independent molecules. Progress of the refinement was monitored by R_{free} (*23*), which was calculated using the same set of reflections used for the R_{free} calculation in the refinement of the native structure. Ordered water molecules were automatically added with the program ARP (*24*). Manual model building was carried out with the program O (*25*). All the active site ligands were well defined in both $2F_o - F_c$ and $F_o - F_c$ maps (Figure 3). The quality of the stereochemical parameters of the refined models was evaluated with PROCHECK (*26*). Data collection and refinement statistics are listed in Table 1.

Analysis and inspection of the three-dimensional structures were carried out with O (*25*) and programs of the Uppsala Software Factory (*27*) and of the CCP4 package (*20*). The solvent accessible surface was calculated with the program Area (*20*) using a probe radius of 1.4 Å. Cutoff distances of 4.0 and of 3.4 Å were used for van der Waals contacts and H-bonds, respectively. Figures were generated with Molscript (*28*), Bobscript (*29*), and Dino (*30*).

RESULTS

Overall Structure. The crystal structure of PAO in the reduced state and in complex with the inhibitors CHENSpm, 1,8-diaminooctane, and guazatine (Figure 1 and Table 1) has been investigated. In all cases, the inhibitors are well defined in the electron density map (Figure 3), being bound in the U-shaped catalytic tunnel that runs across the PAO structure (Figure 2). The crystals of maize PAO contain three enzyme molecules in the asymmetric unit (named A, B, and C). As in the native structure (*14*), chain C has a slightly lower

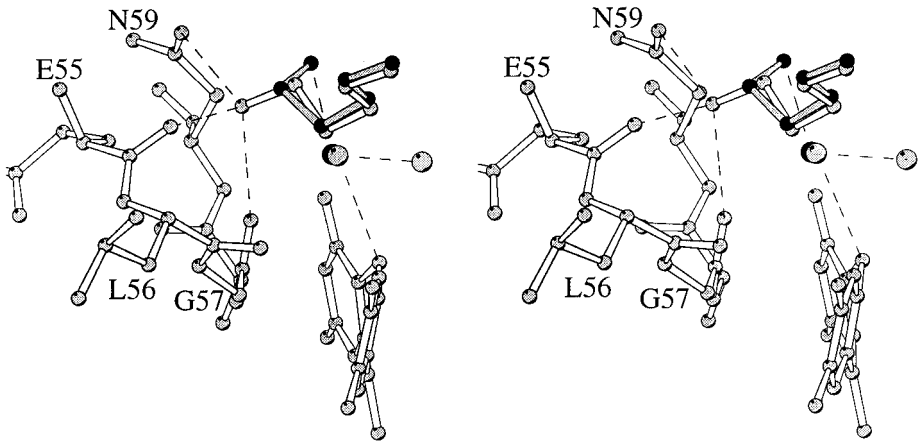

FIGURE 4: Stereoview of the different conformations of Lys300 in oxidized (PDB entry 1b37) and reduced PAO (present study). The water molecule bound to N5 and the side chain of Lys300 in the native oxidized structure are outlined by gray bonds and black atoms. The orientation is the same as in Figure 2.

average *B*-factor with respect to those of the A and B monomers (Table 1). For this reason, chain C has been chosen as the reference molecule for model analysis and structure description. However, in all complexes, the three crystallographically independent monomers, which were subjected to tight NCS restraints throughout the refinement, are virtually identical in both overall structure and geometry of the active center and substrate binding site (Table 1).

Neither cofactor reduction nor inhibitor binding causes significant conformational changes compared to native PAO. The rmsd between equivalent Cα atoms of the native unligated enzyme and the complexes with CHENSpm at pH 4.6, CHENSpm at pH 7.0, 1,8-diaminooctane, and guazatine are 0.13, 0.17, 0.10, and 0.14 Å, respectively. Likewise, the rmsd deviation between the native oxidized enzyme and the reduced protein is 0.27 Å. Given the absence of any change in the overall structure, the description of the PAO·inhibitor complexes will mainly focus on the catalytic center and substrate binding site.

Reduced PAO. Soaking of crystals in a solution containing the substrate spermine led to a change in the color of the crystals from bright yellow, typical of the oxidized enzyme, to a pale color. This change occurred in a few minutes and suggested that the crystalline enzyme reacted with the substrate, thereby becoming reduced. The soaking experiment was carried out in air-saturated solutions, indicating that, despite the presence of oxygen, the large excess of substrate (5 mM) was able to keep crystalline PAO in the reduced state (see ref *31*). Consistent with this observation, transfer of a reduced "colorless" crystal to a substrate free solution resulted in crystal reoxidation as indicated by the almost immediate reappearance of the yellow color. A protective effect against reoxidation brought about by the presence of substrate in excess has been observed in other flavoenzyme crystals such as those of D-amino acid oxidase (*32*, *33*).

The electron density of the reduced enzyme does not show any indication of the presence of active site ligand(s), with the innermost part of the catalytic tunnel being occupied by eight ordered water molecules. Thus, it appears that the products generated by spermine oxidation (Figure 1) are released from PAO after catalysis. The structure of the active site of the reduced enzyme is identical to that of the native oxidized PAO (*14*). The heavily bent conformation of the flavin is left unmodified by reduction, with an angle of 28° between the dimethylbenzene and pyrimidine rings, very close to the value of 30° observed in the oxidized enzyme. The only change observed in the reduced protein affects the Lys300 conformation (Figure 4). In native oxidized PAO, the amino group of Lys300 is engaged in a H-bond with a water molecule, which is further H-bonded to the flavin N5 atom. Upon reduction, the χ_4 torsion angle of Lys300 changes from 69° to −162°, leading to a 1.9 Å shift of the Nϵ amino group. In its new position, Nϵ interacts with the side chain of Asn59 and the backbone oxygen atoms of Glu55 and Gly57. However, despite such a movement of Lys300, the water molecule, which in the oxidized structure is H-bonded to N5 and Lys300, retains its position also in the reduced enzyme. In particular, this water molecule is within H-bonding distance of the flavin N5 atom and another solvent molecule, not present in the oxidized protein.

Upon cofactor reduction, the flavin N5 atom becomes protonated. Lys300 seems to be perfectly positioned to function as a conformational switch that compensates for the change in the flavin protonation state. In the oxidized PAO, a water molecule acts as a bridge between the unprotonated N5 atom and the positively charged Lys300 side chain. After reduction, Lys300 moves away, possibly allowing a reorientation of this water, which, therefore, is enabled to function as a H-bond acceptor in the interaction with the protonated N5 atom of the reduced FAD.

PAO·Guazatine Complex. Guazatine inhibits maize PAO with a K_i value of 7.5×10^{-9} M at pH 6.5 and 25 °C (*34*). Among PAO inhibitors, guazatine comprises the longest linear chain, consisting of two octane units that are connected by a secondary nitrogen atom (N9 in Figure 1). Such a long $(CH_2)_8$-NH-$(CH_2)_8$ chain is further elongated by two terminal guanidinium groups (Figure 1).

Guazatine binds to the catalytic tunnel of PAO (Figure 2), adopting a curved conformation that is made possible mainly by two kinks along the path of the inhibitor chain. In particular, C4−C5−C6−C7, C5−C6−C7−C8, N9−C10−C11−C12, and C10−C11−C12−C13 torsion angles (Figure 5a) have values of −117°, 127°, −110°, and −83°, respectively, being the only dihedral angles of the bound guazatine which do not adopt the anti conformation (angle of ∼180°). Despite the bulkiness of the ligand, the positions of the atoms lining the active site tunnel in the PAO·guazatine complex are strikingly identical to those of the

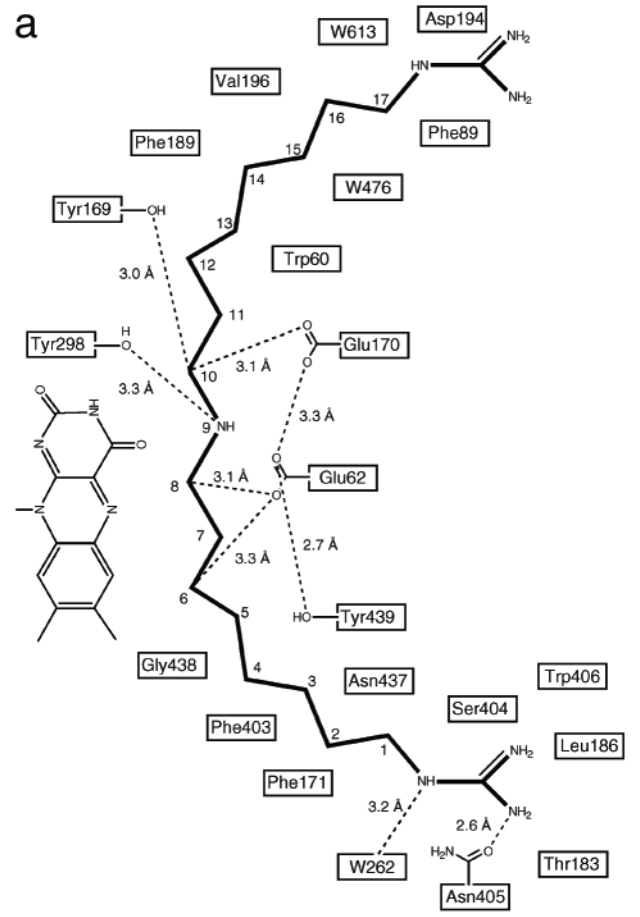

FIGURE 5: (a) Schematic drawing of the PAO·guazatine interactions. H-bonds are indicated with dashed lines. (b) Mode of binding of guazatine to the U-shaped tunnel. The surface of the protein is shown in a semitransparent representation together with a ball-and-stick model of guazatine and FAD (carbon atoms in yellow, nitrogen blue, oxygen red, and phosphorus green). With respect to Figure 2, the protein has been rotated by 120° about a vertical axis, to highlight the location of the inhibitor guanidinium groups at the tunnel openings. In this orientation, the guanidinium group bound to the C17 atom (see Figure 1 and panel a) is in the upper position.

native oxidized structure. The only movement is a small 0.15 Å shift of the carbonyl oxygen of Gly438. Guazatine extensively interacts with PAO (Figure 5a) through van der Waals contacts with aromatic side chains. Moreover, the secondary N9 nitrogen of guazatine is H-bonded to Tyr298, whereas three inhibitor carbon atoms (C6, C8, and C10) are within H-bonding distance of the carboxylate groups of Glu62 and Glu170. The presence of this type of CH···O H-bonds also characterizes the PAO·MDL72527 complex (*14*) and, therefore, seems to be a recurrent feature in the PAO inhibitor binding mode, independent of the nature of the active site ligand.

A remarkable feature revealed by the structure of the PAO·guazatine complex is the fact that the long inhibitor chain completely fills the tunnel (Figure 5b). When complexed to the enzyme, guazatine has a solvent accessible surface area of only 90 Å^2, which can be entirely ascribed to the terminal guanidinium groups located at the tunnel entrances (Figure 5b). By contrast, the total surface area of the guazatine molecule is 720 Å^2, indicating that formation of the PAO·inhibitor complex buries about 90% (630 Å^2) of the guazatine surface area. In keeping with this observation, the inhibitor binding causes the expulsion of all eight ordered water molecules present in the tunnel of the unligated enzyme structure. Thus, the excellent complementarity between the tunnel and guazatine leads to nearly complete desolvation of the bound inhibitor.

PAO·1,8-Diaminooctane Complex. 1,8-Diaminooctane inhibits maize PAO with a K_i of 3.0×10^{-7} M (R. Federico, unpublished). The length of 1,8-diaminooctane is approximately half of that of guazatine (Figure 1), being among the shortest known PAO inhibitors. The electron density map of the PAO·1,8-diaminooctane complex showed a strong and elongated peak in the central part of the tunnel in all three crystallographically independent protein molecules. Surprisingly, the electron density peak turned out to be too long to simply account for one 1,8-diaminooctane ligand, its length being consistent with a chain of about 15 atoms (Figure 6). The electron density could reflect the presence of two adjacent nonoverlapping inhibitor molecules, one or both of them having part of their structure in a disordered conformation, not visible in the electron density map. Although this interpretation of the electron density cannot be completely ruled out, it has been disregarded in view of the following considerations: (i) refinement of two side-by-side 1,8-diaminooctane molecules gave poorer statistics; (ii) as shown by the guazatine complex, the narrow tunnel seems unlikely to give the degree of flexibility required to justify the lack of well-defined electron density for part of one or both of the two bound inhibitors; and (iii) the electron density peak is continuous, which is not expected if two adjacent nonoverlapping inhibitor molecules are bound.

On these bases, the electron density has been instead modeled as two overlapping 1,8-diaminooctane molecules (Figure 6), whose atoms were refined with an occupancy of 0.5. This value was suggested by refinement of the inhibitor occupancies (*21*). This interpretation assumes that 1,8-diaminooctane has at least two binding modes that are mutually exclusive and partly overlapping. In each of the alternative conformations, the terminal amino groups located in the innermost part of the tunnel form H-bonds to the protein, one with Tyr298 and the other with Glu62. The first H-bond mimics the interaction of N9 of guazatine with the tyrosine side chain (Figure 5a), whereas the other H-bond

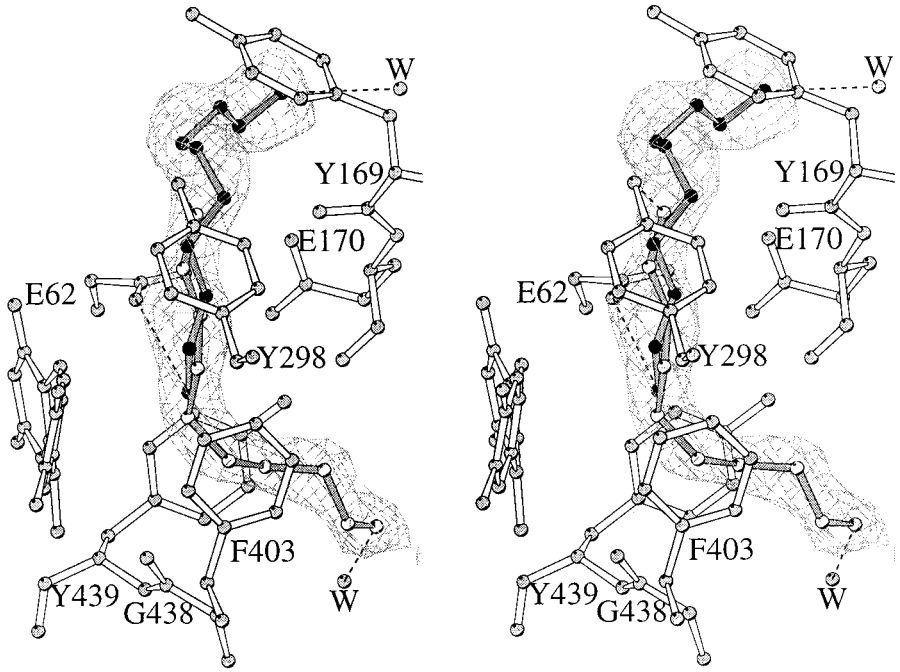

FIGURE 6: Stereoview of the PAO·1,8-diaminooctane complex (chain C). The alternative positions of the two inhibitor molecules are outlined with black and light gray atoms, respectively. H-bonds between the inhibitor amino groups and PAO are indicated with dashed lines. The $2F_o - F_c$ map calculated before the inclusion of the inhibitor atoms in the refinement is shown. The contour level is 0.85σ. The orientation is the same as in Figure 2.

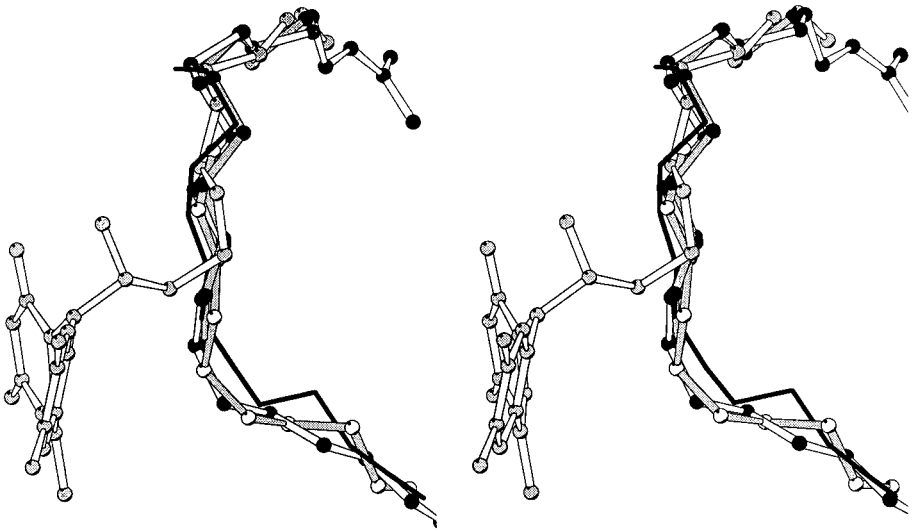

FIGURE 7: Superposition of the PAO·inhibitor complexes. Guazatine and the CHENSpm·flavin adduct have white bonds with the atoms colored in black and gray, respectively. The two 1,8-diaminooctane molecules are outlined with gray bonds as in Figure 6. For comparison, the atomic trace of the MDL72527 inhibitor (PDB entry 1b5q) is shown in black. The orientation is the same as in Figure 2.

mimics that of the C6 atom of guazatine with the glutamate. Indeed, the two alternative conformations of 1,8-diaminooctane closely resemble that of guazatine (Figure 7). Thus, the 1,8-diaminooctane complex is consistent with the idea emerging from the PAO·guazatine structure that the tunnel provides along its entire path a favorable environment for binding aliphatic molecules of variable length.

Covalent PAO·CHENSpm Complex at pH 4.6. Several asymmetrically alkylated polyamine analogues have shown cytotoxic effects on cancer cells and are of potential therapeutic use as antitumor agents (*2*, *8*, *11*). We have investigated PAO in complex with one of these compounds, CHENSpm, which is characterized by an ethyl and a cycloheptyl terminal substituent (Figure 1). When PAO crystals were soaked in a CHENSpm-containing solution, they gradually became colorless. Such a crystal bleaching process required several hours to be completed and suggested that CHENSpm very slowly reacted with the oxidized crystalline protein generating a reduced form of the cofactor. The electron density map, calculated with diffraction data measured from a crystal soaked for 24 h in CHENSpm, confirmed these observations. The electron density was compatible with the presence of a covalent adduct between the C4 atom of CHENSpm (Figure 1) and the flavin N5 atom (Figure 3). The synthesis of this flavin derivative could be triggered by a slow oxidation of the N3−C4 bond of CHENSpm (Figure 8). The resulting imino-CHENSpm product could then undergo hydrolysis, with release of

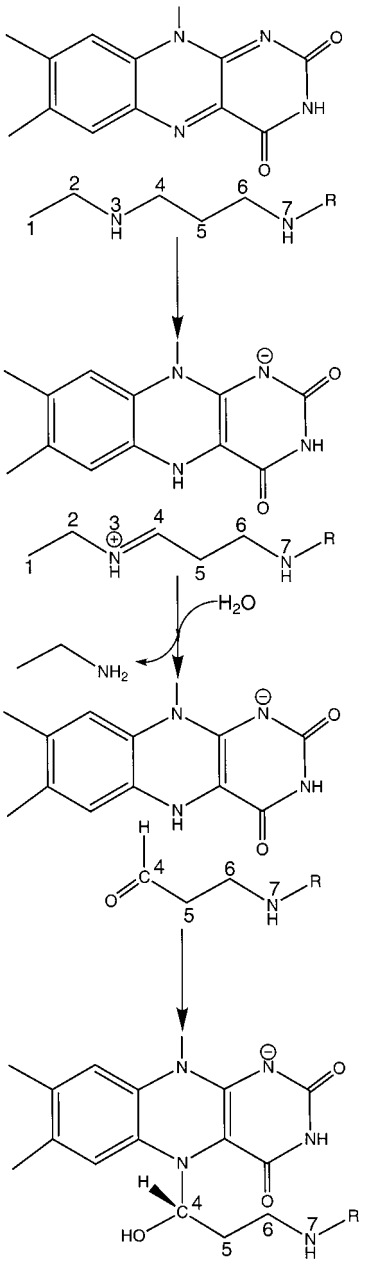

FIGURE 8: Scheme for the proposed reaction leading to the formation of the PAO·CHENSpm covalent adduct. The CHENSpm atoms are numbered as in Figure 1.

aminoethane and formation of a transient complex between the reduced enzyme and the CHENSpm-derived aldehyde. The latter could then react with the reduced flavin, leading to the formation of the observed covalent adduct. A very similar mechanism involving a reduced PAO−aldehyde intermediate with formation of a covalent flavin derivative has been shown to exist in the reaction of lactate oxidase with glycolate (*35*), and therefore, it is not unprecedented in flavoenzymology.

Several lines of evidence support the presence of the proposed covalent adduct. The electron density unambiguously shows that the atom covalently linked to N5 has a nonplanar configuration. This is fully consistent with the tetrahedral configuration of the adduct C4 atom carrying a hydroxyl group (Figure 8). Moreover, strong electron density departs from the flavin N5 locus extending across one arm of the U-shaped catalytic tunnel (the "upper" arm in Figures 2 and 5b). The CHENSpm linear chain going from C4 to C16 fits very well this elongated density peak (Figure 3). Chains A and B lack any residual electron density for the cycloheptyl moiety. This group falls in a position outside the tunnel and, therefore, may not be fixed in a defined conformation. Interestingly, in chain C, there is a residual density, which extends from the C16 position (Figure 3) and might reflect the presence of a partly ordered cycloheptyl ring. However, this density is too weak and poorly defined to allow modeling of the CHENSpm terminal substituent.

In the covalent adduct, the CHENSpm chain protruding from the flavin binds in one of the two arms of the U-shaped tunnel. Its position overlaps that of the N9−C17 segment of guazatine (Figures 5a, 5b, and 7). Conversely, the other arm remains occupied by a few ordered solvent molecules. Thus, it could easily provide access of the water molecule involved in the hydrolysis of imino-CHENSpm and allow the subsequent release of the aminoethane product (Figure 8). In agreement with the other PAO·inhibitor structures, the covalent adduct also displays virtually no conformational changes with respect to the native enzyme. The isoalloxazine ring is in the usual bent conformation, identical to that of the native protein (Figure 3). Moreover, the flavin N5 atom is within H-bonding distance of a water molecule, which is additionally H-bonded to the hydroxyl group of the CHENSpm C4 atom (Figure 3). The only significant change affects Lys300, whose side chain adopts the same conformation observed in the reduced enzyme (Figure 4). This feature, however, is not surprising, reflecting the reduced state of the flavin in the PAO·CHENSpm derivative.

Covalent PAO·CHENSpm Complex at pH 7.0. A soaking experiment using CHENSpm was carried out in a solution buffered by 100 mM BES (pH 7.0) instead of sodium acetate (pH 4.6), which was employed in all other soaking experiments. Despite the relatively large pH change, PAO crystals maintained their diffraction power and a 2.0 Å data set could be measured. The resulting electron density map turned out to be virtually indistinguishable from that calculated for the PAO·CHENSpm complex at pH 4.6. Indeed, after refinement, the rmsd between the Cα atoms of the PAO·CHENSpm structures at pH 7.0 and pH 4.6 is 0.08 Å for all three NCS-related molecules. This fact leads to three main conclusions: (i) PAO confirms to have a quite rigid structure; (ii) the acidic pH used for crystal growth and analysis is very unlikely to perturb the protein structure with respect to that adopted by the enzyme at neutral pH, reflecting the ability of maize PAO to retain catalytic activity over a wide pH range (*36*); and (iii) formation of the covalent adduct also occurs at neutral pH.

DISCUSSION

Lock-and-Key Inhibitor Binding in PAO. The crystallographic investigation of PAO·inhibitor complexes reveals a precise complementarity between the catalytic tunnel and the active site ligands. The conformation of the protein is unaffected by the inhibitors, whose binding mode appears, therefore, to be of the lock-and-key type with little or no induced fit. Indeed, in all complexes, water molecules are totally removed from the tunnel section where the ligand is positioned, effectively desolvating the PAO-bound ligand. These features are well exemplified by the complex with guazatine (Figure 2). Except for the guanidinium terminal

groups, all inhibitor atoms become solvent inaccessible with the burial of more than 600 Å^2 of surface area. The long guazatine chain contains 18 dihedral angles (Figure 5a), which, on binding, become fixed in a single conformation. The entropic cost of such a "conformational freezing" is compensated by the extensive guazatine−protein interactions, most of them involving inhibitor aliphatic carbons and aromatic side chains. Thus, the hydrophobic effect due to the removal of the inhibitor aliphatic moieties from aqueous solvent seems to provide the main factor in the binary complex stabilization.

However, the PAO·inhibitor interactions do not simply involve van der Waals contacts but also CH···O H-bonds (Figure 5a). Therefore, it appears that the interactions with water molecules that the ligand can establish in solution are partly replaced in the enzyme·inhibitor complexes by H-bonds with protein oxygen atoms. This phenomenon may reflect the fine energetic balancing that PAO must effect in substrate binding. The tunnel provides a solvent-protected hydrophobic environment that is favorable for the aliphatic segments of the substrates. On the other hand, an entirely hydrophobic binding site may represent an "overly favorable" environment, which could form an energetic trap, hampering catalysis by preventing product(s) release or even formation of the transition state (*37*). PAO avoids this problem by interacting with the substrate through a combination of hydrophobic contacts, which are not possible in solution, and polar CH···O bonds, which are similar to the interactions possibly made in solution by the substrate carbon atoms with the surrounding waters.

An "Out-of-Register" Mechanism of PAO Inhibition. The physiological substrates of PAO bear both primary and secondary amino groups (Figure 1). A remarkable feature revealed by the crystal structure of PAO binary complexes is that the polycationic nature of the polyamine substrates does not find a counterpart in an array of negatively charged residues in the binding site. Indeed, the only group inside the tunnel, which is likely to carry a negative charge, is the Glu62−Glu170 pair, whose side chains are within H-bonding distance from each other (Figures 5a and 9). This feature is related to another important observation emerging from the comparison of the various PAO complexes (Figure 7). Superposition of the PAO-bound inhibitors shows that carbon and nitrogen atoms can bind at the same location within the tunnel. In fact, the positions of the N1 and N8 atoms of a PAO-bound 1,8-diaminooctane overlap those of C15 and C6 of guazatine, respectively. Likewise, N7 of CHENSpm (Figure 3) occupies the same position of guazatine C13. Apparently, the PAO tunnel does not contain subsites, which are specific for amino groups. Rather, either CH_2 or NH atoms, depending on the inhibitor complex, may occupy the same position.

The fundamental question raised by these observations concerns the nature of the structural determinants that discriminate between an actual substrate and an inhibitor of PAO. For example, guazatine (Figure 1) and MDL72527 (*14*) both carry a secondary amino group but, nevertheless, are not oxidized by the enzyme. Inspection of the PAO·inhibitor complexes shows that the ligand secondary amino groups and the adjacent carbon atoms are too far from the reactive N5 locus of the flavin to undergo oxidation. The C8 and C10 atoms of guazatine linked to the N9 secondary amino group (Figures 1 and 5a) are 4.7 and 6.2 Å from N5, respectively. Independent of the exact mechanism of catalysis, these distances are too long to allow flavin-catalyzed oxidation. Thus, it appears that a key factor in achieving catalysis is the correct alignment of the C−N bond undergoing oxidation with respect to the flavin ring. Inhibitors such as guazatine attain an out-of-register binding mode, which allows tight binding but not catalysis.

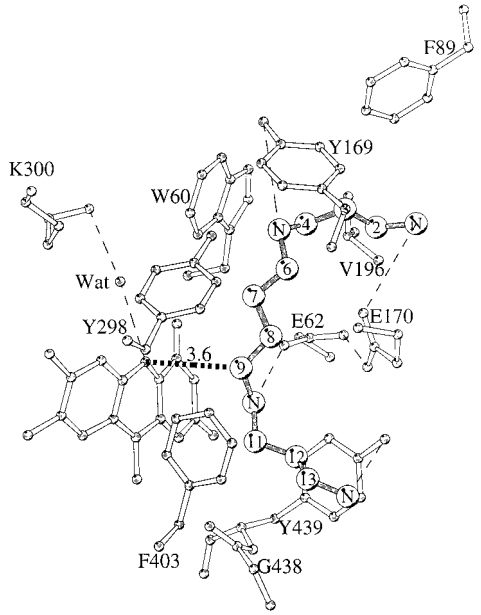

FIGURE 9: Model for spermine binding. Carbon atoms are numbered as in Figure 1. The N5-bound water molecule is labeled with "Wat". The thick dashed line connects the flavin N5 locus and the spermine C9 atom, which undergoes oxidation. The orientation is the same as in Figure 2.

A Model for Spermine Binding. To investigate the structural basis of substrate specificity, the substrate spermine has been tentatively modeled in the PAO active site (Figure 1), based on the following criteria. (i) Guazatine has been used as an atomic skeleton. This inhibitor is very well defined in electron density, and apart from the terminal guanidinium groups, its chain, like spermine, does not contain double bonds (Figure 1). (ii) The position of the site of oxidative attack (spermine C9 in Figure 1) was assumed to be identical to that found in other flavoenzymes. A comparison among flavoprotein structures carrying out dehydrogenation reactions has shown that the CH group undergoing oxidation with concomitant rupture of the C−H bond is located in a strikingly conserved position in front of the N5 locus of the flavin (*15*). The C7 atom of guazatine (Figure 5a) is 3.6 Å from N5 with a C7(guazatine)−N5(flavin)−N10(flavin) angle of 96°, well within the range of values found for the site of oxidative attack in other flavoenzymes (*15*). Thus, the spermine C9 atom (Figure 1) undergoing oxidation in maize PAO was modeled at the same position of guazatine C7.

The PAO·spermine model is shown in Figure 9. As expected, the substrate becomes completely solvent inaccessible when bound to the protein. The substrate amino groups are all within H-bonding distance of protein side chains: N1 from Glu170, N5 from Tyr169, N10 from Glu62, and N14 from Tyr439. In this H-bond network, Glu62 and Glu170 are crucial in that they bind to primary (N1) and

secondary (N10) amino groups of spermine, respectively. The Glu62−Glu170 pair may represent the structural element that senses the correct spacing between the substrate primary and secondary amino groups and properly aligns the substrate within the tunnel to achieve catalysis. However, the role of these residues in dictating substrate specificity needs to be tested by site-directed mutagenesis.

The mechanism of flavin-dependent oxidation of amines has been thoroughly investigated, especially for monoamine oxidase (see ref *38* and references therein) and sarcosine oxidase (*39*). In particular, monoamine oxidase is considered the prototype of amine oxidases; its sequence is 20% identical to that of PAO (*14*), although it acts on primary rather than secondary amines. Three mechanisms have been proposed for monoamine oxidase and sarcosine oxidase (*38*, *39*): (i) a single electron-transfer mechanism involving an intermediate flavin anion/amine cation radical pair, (ii) a polar nucleophile mechanism occurring via a nucleophilic attack at flavin C4a by a deprotonated amine, and (iii) a hydride transfer mechanism requiring direct transfer of a hydride ion to flavin N5 from the substrate carbon adjacent to the amino group. The available structural data for PAO do not discriminate between these hypothetical mechanisms. The side chain of Glu62 and the water molecule H-bonded to flavin N5 are well positioned to play a role in catalysis, e.g., to abstract a proton from the substrate. Moreover, in the proposed model for spermine binding, the substrate N10 and C9 atoms are juxtaposed to flavin C4a and N5, respectively. This situation is compatible with any of the three catalytic mechanisms that have been proposed. In fact, it would make possible transfer of an electron or of a hydride to the flavin as predicted by the single-electron transfer and hydride transfer mechanisms, respectively. However, this substrate binding mode is compatible also with the formation of the covalent C4a adduct postulated by the nucleophile mechanism. Interestingly, the orientation with respect to the flavin of the spermine N10−C9 bond undergoing oxidation is highly similar to that observed in D-amino acid oxidase for the N−Cα unit of the amino acid substrate (*40*). Thus, an intriguing hypothesis is that the structural features underlying substrate oxidation among flavin-dependent amino acid oxidases and amino oxidases may be similar.

CONCLUSIONS

The narrow catalytic tunnel of PAO is highly complementary to inhibitors and substrates. However, except for the Glu62−Glu170 pair, in the tunnel there are no other negatively charged residues that take part in the recognition of the ligand amino groups. This is in sharp contrast to other polyamine binding proteins, such as deoxyhypusine synthase (*41*) and the polyamine carrier protein PotD (*42*), where the primary amino groups of spermidine are bound through interactions with several Asp and Glu residues. In vivo, PAO is known to act on spermine, spermidine, N^1-acetylspermine, N^1-acetylspermidine, and, in certain organisms, even norspermine (*1*, *5*). The lack of charged groups in the PAO catalytic tunnel may serve the purpose of conferring to the enzyme a rather broad specificity, allowing the recognition of ligands with a variable length and number of amino groups. These differences in the architecture of the substrate binding sites among proteins acting on polyamines may be exploited for the design of inhibitors targeting specific enzymes involved in polyamine metabolism.

ACKNOWLEDGMENT

We thank M. Rizzi (Università di Pavia) for many stimulating discussions. The supervision of the ESRF and EMBL/DESY staff during synchrotron data collection is gratefully acknowledged. Access to the EMBL Hamburg facility is supported by the European Union program HPRI (Contract HPRI-CT-1999-00017). CHENSpm was a kind gift from R. A. Casero, Jr. (University of Baltimore).

REFERENCES

1. Tabor, C. W., and Tabor, H. (1984) *Annu. Rev. Biochem. 53*, 749−790.
2. Pegg, A. E., and Hu, R. H. (1995) *Cancer Lett. 95*, 247−252.
3. Igarashi, K., and Kashiwagi, K. (2000) *Biochem. Biophys. Res. Commun. 271*, 559−564.
4. Federico, R., and Angelini, R. (1991) in *Biochemistry and Physiology of Polyamines in Plants* (Slocum, R. D., and Flores, H. E., Eds.) pp 41−56, CRC Press, Boca Raton, FL.
5. Seiler, N. (1995) *Prog. Brain Res. 106*, 333−344.
6. Federico, R., Cona, A., Angelini, R., Schininà, M. E., and Giartosio, A. (1990) *Phytochemistry 29*, 2411−2414.
7. McCloskey, D. E., Woster, P. M., Casero, R. A., Jr., and Davidson, N. E. (2000) *Clin. Cancer Res. 6*, 17−23.
8. Marton, L. J., and Pegg, A. E. (1995) *Annu. Rev. Pharmacol. Toxicol. 35*, 55−91.
9. Hu, R. H., and Pegg, A. E. (1997) *Biochem. J. 328*, 307−316.
10. Schipper, R. G., Penning, L. C., and Verhofstad, A. A. (2000) *Semin. Cancer Biol. 10*, 55−68.
11. Ha, H. C., Woster, P. M., Yager, J. D., and Casero, R. A., Jr. (1997) *Proc. Natl. Acad. Sci. U.S.A. 94*, 11557−11562.
12. Laurenzi, M., Rea, G., Federico, R., Tavladoraki, P., and Angelini, R. (1999) *Planta 208*, 146−154.
13. Tavladoraki, P., Schinina, M. E., Lecconi, F., Di Agostino, S., Manera, F., Rea, G., Mariottini, P., Federico, R., and Angelini R. (1998) *FEBS Lett. 426*, 62−66.
14. Binda, C., Coda, A., Angelini, R., Federico, R., Ascenzi, P., and Mattevi, A. (1999) *Structure 7*, 265−276.
15. Fraaije, M. W., and Mattevi, A. (2000) *Trends Biochem. Sci. 25*, 126−132.
16. Woster, P. M. (1995) in *Polyamines: Regulation and Molecular Interaction* (Casero, R. A., Ed.) pp 171−186, Landes, Austin, TX.
17. Binda, C., Coda, A., Angelini, R., Federico, R., Ascenzi, P., and Mattevi, A. (1998) *Acta Crystallogr. D54*, 1429−1431.
18. Rodgers, D. W. (1994) *Structure 2*, 1135−1140.
19. Leslie, A. G. (1999) *Acta Crystallogr. D55*, 1696−1702.
20. Collaborative Computational Project Number 4 (1994) *Acta Crystallogr. D50*, 760−767.
21. Tronrud, D. E., Ten Eyck, L. F., and Matthews, B. W. (1987) *Acta Crystallogr. A43*, 489−501.
22. Berman, H. M., Westbrook, J., Feng, Z., Gilliland, G., Bhat, T. N., Weissig, H., Shindyalov, I. N., and Bourne, P. E. (2000) *Nucleic Acids Res. 28*, 235−242.
23. Brünger, A. T. (1992) *Nature 355*, 472−475.
24. Perrakis, A., Morris, R., and Lamzin, V. S. (1999) *Nat. Struct. Biol. 5*, 458−463.
25. Jones, T. A., Zou, J. Y., Cowan, S. W., and Kjeldgaard, M. (1991) *Acta Crystallogr. A47*, 110−119.
26. Laskowski, R. A., MacArthur, M. W., Moss, D. S., and Thornton, J. M. (1993) *J. Appl. Crystallogr. 26*, 283−291.
27. Kleywegt, G. J., and Jones, T. A. (1994) *Acta Crystollogr. D50*, 178−185.
28. Kraulis, P. J. (1991) *J. Appl. Crystallogr. 24*, 946−950.
29. Esnouf, R. M. (1999) *Acta Crystallogr. D55*, 938−940.
30. Philippsen, A. (1999) *Dino: Visualising Structural Biology* (http://www.bioz.unibas.ch/∼xray/dino).

31. Bellelli, A., Angelini, R., Laurenzi, M., and Federico, R. (1997) *Arch. Biochem. Biophys. 343*, 146−148.
32. Todone, F., Vanoni, M. A., Mozzarelli, A., Bolognesi, M., Coda, A., Curti, B., and Mattevi, A. (1997) *Biochemistry 36*, 5853−5860.
33. Miura, R., Setoyama, C., Nishina, Y., Shiga, K., Mizutani, H., Miyahara, I., and Hirotsu, K. (1997) *J. Biochem. 122*, 825−833.
34. Federico, R., Leone, L., Botta, M., Binda, C., Angelini, R., Venturini, G., and Ascenzi, P. (2000) *J. Enzyme Inhib.* (in press).
35. Ghisla, S., and Massey, V. (1980) *J. Biol. Chem. 255*, 5688−5696.
36. Federico, R., Alisi, C., and Forlani, F. (1989) *Phytochemistry 28*, 45−50.
37. Warshel, A. (1998) *J. Biol. Chem. 273*, 27035−27038.
38. Miller, J. R., and Edmondson, D. E. (1999) *Biochemistry 38*, 13670−13683.
39. Wagner, M. A., Trickey, P., Chen, Z. W., Mathews, F. S., and Jorns, M. S. (2000) *Biochemistry 39*, 8813−8824.
40. Umhau, S., Pollegioni, L., Molla, G., Diederichs, K., Welte, W., Pilone, M. S., and Ghisla, S. (2000) *Proc. Natl. Acad. Sci. U.S.A. 97*, 12463−12468.
41. Liao, D.-I., Wolff, E. C., Park, M. H., and Davies, D. R. (1998) *Structure 6*, 23−32.
42. Sugiyama, S., Vassylyev, D. G., Matsushima, M., Kashiwagi, K., Igarashi, K., and Morikawa, K. (1996) *J. Biol. Chem. 271*, 9519−9525.

BI002751J